How to cite: Angew. Chem. Int. Ed. 2024, e202406843
doi.org/10.1002/anie.202406843

Fluorescent Probes | Very Important Paper

Enzymes in Synergy: Bacteria Specific Molecular Probe for Locoregional Imaging of Urinary Tract Infection in vivo

Evelias Yan Hui Xin[+], Germain Kwek[+], Xiaoyu An[+], Caixia Sun, Songhan Liu, Ng Shuang Qing, Shonya Lingesh, Lai Jiang, Gang Liu, and Bengang Xing**

Abstract: Uropathogenic *Escherichia coli* (UPECs) is a leading cause for urinary tract infections (UTI), accounting for 70–90 % of community or hospital-acquired bacterial infections owing to high recurrence, imprecision in diagnosis and management, and increasing prevalence of antibiotic resistance. Current methods for clinical UPECs detection still rely on labor-intensive urine cultures that impede rapid and accurate diagnosis for timely UTI therapeutic management. Herein, we developed a first-in-class near-infrared (NIR) UPECs fluorescent probe (NO–AH) capable of specifically targeting UPECs through its collaborative response to bacterial enzymes, enabling locoregional imaging of UTIs both in vitro and in vivo. Our NO–AH probe incorporates a dual protease activatable moiety, which first reacts with OmpT, an endopeptidase abundantly present on the outer membrane of UPECs, releasing an intermediate amino acid residue conjugated with a NIR hemicyanine fluorophore. Such liberated fragment would be subsequently recognized by aminopeptidase (APN) within the periplasm of UPECs, activating localized fluorescence for precise imaging of UTIs in complex living environments. The peculiar specificity and selectivity of NO–AH, facilitated by the collaborative action of bacterial enzymes, features a timely and accurate identification of UPECs-infected UTIs, which could overcome misdiagnosis in conventional urine tests, thus opening new avenues towards reliable UTI diagnosis and personalized antimicrobial therapy management.

Introduction

Urinary tract infections (UTI) remain as the most prevalent infectious diseases encountered in clinical practice worldwide. Nearly half of our population may experience at least one symptomatic UTI during their lifetime, with a severe concern for recurrence within six months from the point of original infection, affecting 150 million individuals annually with considerable morbidity and high medical costs.[1] Among various uropathogens associated to UTI development,[2] about 70–90 % of community-acquired UTIs are predominantly infected by uropathogenic *Escherichia coli* (UPECs), with their virulence actively involved in pathogenic adhesion, invasion and resistance to host immune defense and metabolic pathways.[3] Moreover, UPECs could implement their protective niches against host surveillance, antibiotic perturbation, and importantly, clearance by micturition.[4] Conventional strategies for diagnosing UTIs involve standard urine cultures and bacterial isolation, which are both time-consuming and labour intensive.[4,5] Within such long turnaround time for analysis, patients are often prescribed empirical antibiotics instead without a proper diagnosis of their UTI, thus aggravating high risk of extensive spread of antibiotic-resistance.[5] Furthermore, urine cultures are not always routinely performed as discouraged by guidelines worldwide, mostly due to the concerns of imprecise diagnosis, delayed therapy and antibiotic resistance.[6] Although molecular and immunological diagnosis methods including engineered phage, genetic editing and amplification, as well as antibody-mediated strain enrichment etc[7] enabled quantitative uropathogen sensing, these operations are usually costly and complex to

[*] E. Y. H. Xin,[+] Dr. G. Kwek,[+] Dr. C. Sun, S. Liu, N. S. Qing, S. Lingesh, Prof. Dr. B. Xing
School of Chemistry, Chemical Engineering and Biotechnology
Nanyang Technological University
21 Nanyang Link, S637371 Singapore (Singapore)
E-mail: Bengang@ntu.edu.sg

X. An,[+] Prof. Dr. L. Jiang, Prof. Dr. G. Liu
State Key Laboratory of Vaccines for Infectious Diseases, Center for Molecular Imaging and Translational Medicine, Xiang An Biomedicine Laboratory, National Innovation Platform for Industry-Education Integration in Vaccine Research, School of Public Health
Xiamen University
4221 Xiangan Road, Xiang'an District, Xiamen, Fujian, 361102
China
E-mail: Gangliu.cmitm@xmu.edu.cn

X. An,[+] Prof. Dr. G. Liu
State Key Laboratory of Cellular Stress Biology, School of Life Sciences
Xiamen University
4221 Xianganan Road, Xiang'an District, Xiamen, Fujian, 361102
China

Prof. Dr. L. Jiang
School of Pharmaceutical Sciences
Zhejiang Chinese Medical University
260 Baichuan Road, Fuyang District, Hangzhou, Zhejiang, 311402
China

[+] These authors contributed equally.

implement in limited healthcare settings.[8] As such, a simple, rapid, and accurate strategy that can directly identify UTI caused by UPECs to establish an effective therapeutic management with minimal prescription of broad-spectrum antibiotics, is of high necessity in clinics.[4,9]

Outer membrane protease T (OmpT), a family of bacterial endopeptidase tightly embedded in the outer membrane of UPECs, has been recognized as critical virulence factors implicated for UTI pathogenesis.[10] Throughout uropathogenic adhesion and invasion of UPECs, OmpT functions as a defence mechanism by cleaving cationic antimicrobial peptides (AMPs) secreted by host epithelial cells, making UPECs more resistant to defensive AMPs than commensal *E. coli* strains.[10b] OmpT specifically cleaves at consecutive basic residues in the sequence: $-P_n-R\downarrow(R/K)-P_n'-$ (whereby, $n=1$, 2, or n, and P or P' represents amino acid, respectively).[10,11] To date, the unique proteolytic hydrolysis of OmpT has been utilized for MS identification of post-translation modifications, mutational screening of enzyme variants on cell surface and bio-sensing of food- and water-borne pathogen contamination.[11] However, the exact roles of OmpT in the innate defence and pathogenesis of UTI remains elusive. Such peculiar defence and virulence mechanism inspired us to exploit its characteristics enzymatic activity to develop a unique and reliable strategy for specific identification of UPECs in intricate living conditions, thus greatly facilitating prompt and accurate diagnosis of UPECs pathogenesis at the region of UTI and enabling effective and proper treatment.

Herein, we designed a novel near-infrared OmpT-APN hemicyanine (NO–AH) fluorescence probe for specific and regionally targeted imaging of urinary tract infection both in vitro and in vivo (Scheme 1). Our NO–AH probe composed of a peptide sequence containing positive charges, along with two unnatural D-Phe residues with main aims to enhance the structure stability, and importantly, a proteolytic site of *Arg-Arg*, (Ac–Arg-D-Phe-D-Phe–Arg–Arg–), flanked by a NIR hemicyanine fluorophore[12] conjugated at the C-terminus via a self-immolative *para*-aminobenzylalcohol (PABA) group as a spacer.[13] Upon initial peptide affinity to the surface of UPECs, and selective proteolytic cleavage by the outer membrane OmpT protease, the Arg-conjugated hemicyanine fragment (R–CyOH) can be first released. The liberated R–CyOH species will be then recognized by periplasmic exopeptidase, aminopeptidase (APN),[14] which efficiently cleaved off the Arg residue and trapped the activated NIR hemicyanine (CyOH) fluorescence within the UPECs periplasm, enabling localized and real-time UTI imaging caused by UPECs in vitro and in vivo. Such unique responsiveness of bacterial enzymes to the probe localization provides valuable insights for rapid and precise UTI diagnosis in real-life conditions, therefore greatly facilitating their timely and effective antibiotic therapeutic management in clinical practice.

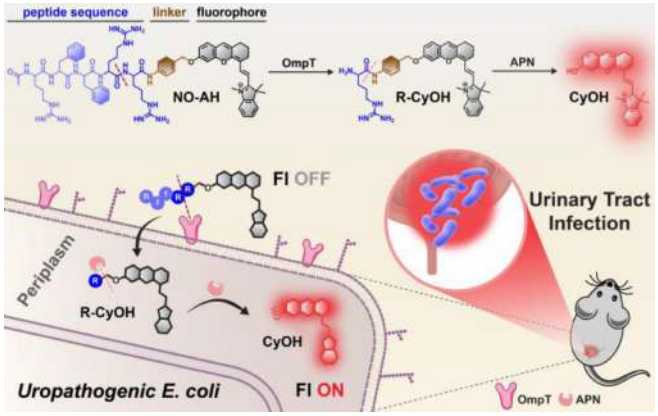

Scheme 1. Schematic illustration of the collaborative activation of NO–AH by intrinsic OmpT and APN enzymes in the presence of urinary tract infection (UTI) caused by uropathogenic *E. coli* (UPECs).

Results and Discussion

Rational Design and Characterization of NO–AH

We first prepared our fluorescent peptide probe (NO–AH) by coupling the NIR hemicyanine moiety with OmpT-APN peptide substrates (Scheme 1 and Figure S2, Supporting Information). Briefly, the OmpT-APN peptide was produced by solid phase peptide synthesis. Then, a self-immolative PABA linker was used to integrate the NIR hemicyanine, (CyOH), with the peptide sequence. The final product NO–AH probe was purified by high performance liquid chromatography (HPLC) and further characterized by mass spectrometry and nuclear magnetic resonance (see the Supporting Information for details).

Next, we evaluated the stability of NO–AH in a buffer solution (Figure S3). The measurement revealed a relatively consistent absorbance and fluorescence intensity after 24 hours, indicating no obvious degradation of NO–AH. We further examined the optical properties of NO–AH and its reactivity towards the synergistic proteolysis of OmpT and APN. As illustrated in Figure 1, NO–AH (10 μM) itself exhibited two characteristic absorption peaks at 604 and 654 nm respectively (Figure 1b), while a simultaneous incubation of NO–AH with OmpT and APN led to a red shift in absorbance (Figure 1b). Moreover, there was a significant fluorescence enhancement observed (~3 folds) at 720 nm when incubated with both enzymes (Figure 1c). As controls, minimal absorbance shift was observed for NO–AH upon individual treatments by OmpT or APN (Figure S4a). Similarly, less fluorescence enhancement was found upon NO–AH incubation with individual enzyme (Figure S4b). These optical responses clearly ascertained the need for simultaneous cleavage of OmpT and APN to give a full fluorescence enhancement of NO–AH.

Additionally, similar bacterial enzyme reactions towards NO–AH were monitored with high-performance liquid chromatography (HPLC). As shown in Figure 1d, we first incubated NO–AH (10 μM) with both OmpT and APN, two peaks appeared at 9.2 mins, corresponding to the R–CyOH substrate itself, and 12.8 mins, attributing to the CyOH molecule. Moreover, we also validated the sequential cleavage effect by both enzymes through HPLC analysis. In

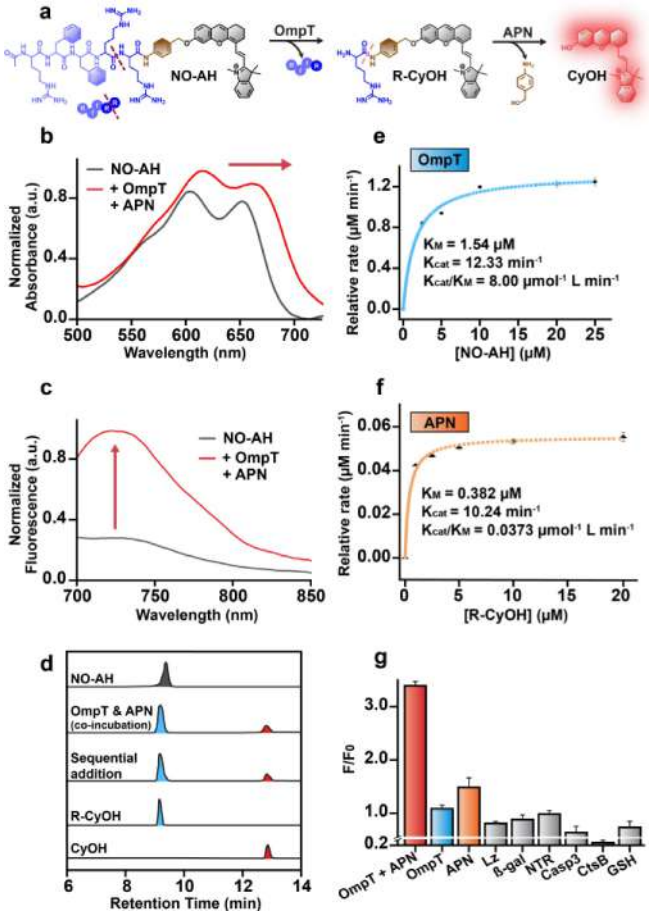

Figure 1. In vitro characterization of NO–AH. (a) Schematic visualization of the enzymatic cleavage of OmpT and APN with NO–AH. (b–c) Absorbance and fluorescence spectra of NO–AH (10 μM) in the presence and absence of both OmpT and APN for 2 h at 37 °C in PBS (pH 7.4). (λ_{ex}: 660 nm) (d) HPLC analysis of OmpT and APN with NO–AH incubated for 2 h at 37 °C in PBS (pH 7.4). (e) Enzyme kinetics of OmpT with NO–AH (10 μM). (f) Enzyme kinetics of APN with R–CyOH (10 μM). (g) The selectivity analysis towards enzymatic NO–AH reaction (10 μM) after incubation with indicated biomolecules for 2 h at 37 °C in PBS. (λ_{ex}: 660 nm; λ_{em}: 720 nm). (F represents the Fluorescence emission of indicated biomolecules at λ_{em}: 720 nm; F0 represents the baseline fluorescence of NO–AH at λ_{em}: 720 nm) Data presented as means ± SD ($n = 3$)

Figure 1d, we first incubated NO–AH with OmpT for 30 mins, a new peak with a retention time of 9.2 mins was observed which was the same as the R–CyOH substrate itself, corroborating the formation of R–CyOH upon OmpT cleavage. Subsequently, we added APN into the same mixture and incubated for another 90 minutes, and a new peak was observed with a retention time of 12.8 mins, attributed to the CyOH molecule, signifying the release of CyOH from R–CyOH after APN proteolysis. As controls, we separately incubated the individual enzymes with NO–AH probe. In Figure S5, incubation of OmpT with NO–AH gave a peak at 9.2 mins, indicating the enzyme cleavage and R–CyOH formation. However, direct incubation of APN with NO–AH could not hydrolyze probe molecule structure to CyOH and a HPLC peak with a retention time of 9.4 mins could be observed, closed to that of the NO–AH probe itself. These results clearly demonstrated the collaborative activation of dual enzymes towards NO–AH recognition. Further analysis of the enzyme kinetics of OmpT to NO–AH, and APN with R–CyOH were also monitored with HPLC, respectively. Within 5 minutes, the NO–AH molecules were facilely cleaved to form R–CyOH when incubated with OmpT. The kinetic constants were calculated with the results showing $K_M = 1.54$ μM and $K_{cat} = 12.33$ min^{-1} (Figure 1e and Figure S6a). Meanwhile, within 2 hours, R–CyOH substrates could be cleaved by APN to release CyOH, yielding reasonable kinetic constants of $K_M = 0.382$ μM and $K_{cat} = 10.24$ min^{-1} (Figure 1f and Figure S6b). These results suggested the promising capability for each enzyme, OmpT and APN, to selectively recognize its respective substrates, NO–AH and R–CyOH, in buffer solution.

Lastly, we analyzed the enzymatic selectivity of NO–AH by individually screening OmpT and APN together with several commonly used biomolecules and components[15] such as lysozyme (Lz), beta-galactosidase (β-Gal), nitroreductase (NTR), caspase 3 (Casp3), cathepsin B (CtsB) and gluthathione (GSH) etc. As shown in Figure 1g, incubation with these common biomolecules showed negligible fluorescence enhancement. Although some non-specific signals observed after individual interactions with OmpT or APN, our NO–AH probe still exhibited promising selectivity towards the sequential activation of bacterial enzymes of OmpT and APN.

Specific and Selective Fluorescence Bacterial Imaging towards Uropathogenic E. coli

Encouraged by the dual enzyme-responsive properties of NO–AH, we investigated the imaging feasibility of NO–AH for potential performance in various live bacterial cultures. In this study, *E. coli* CFT073, *E. coli* UTI89 and *E. coli* J96, three types of uropathogenic *E. coli* strains, with high expression of OmpT, were chosen as our targeted pathogens.[16] In contrast, methicillin-resistant *Staphylococcus Aureus* (MRSA), *Enterococcus Faecalis* (*E. faecalis*) and *Proteus Mirabilis* (*P. mirabilis*) were selected as controls, whereby they are typically reported pathogenic bacteria species that do not contain OmpT. Upon incubation with NO–AH (10 μM), the live bacteria cultures were subjected to confocal microscopy for fluorescent imaging analysis.[17]

As shown in Figure 2a and 2b, strong fluorescence signals were clearly observed in CFT073, UTI89 and J96 strains as compared to others that were deficient in OmpT. As a negative control, NO–AH probe was also incubated with *E. coli* strains such as BL21, a commonly used *E. coli* strain lacking OmpT expression on its outer membrane. As expected, minimal fluorescence was observed in *E. coli* BL21 (Figure S7a and S7b, Supporting Information). These optical images clearly demonstrated impressive imaging capability of NO–AH, with an exceptional selectivity towards UPECs expressing OmpT.

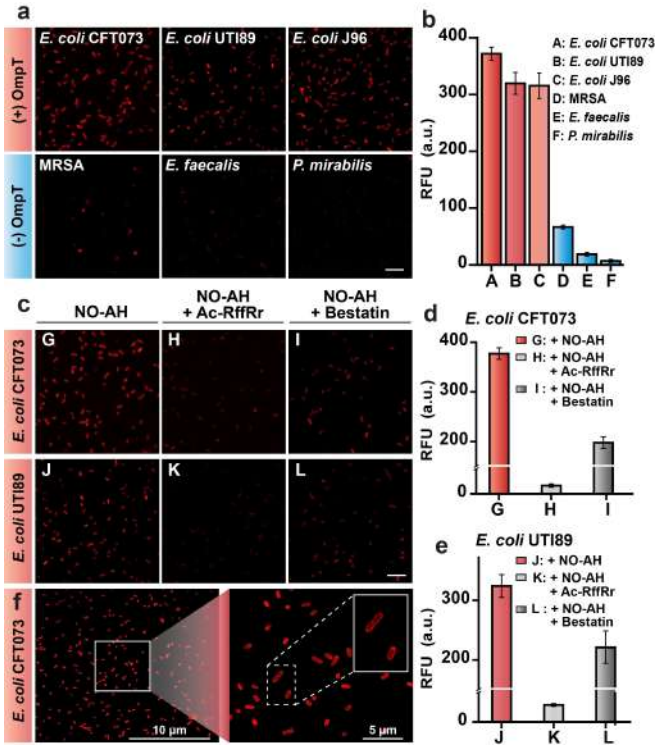

Figure 2. In vitro fluorescence bacteria (~10^8 CFU/mL) confocal microscopy analysis of various bacteria strains after incubation with NO–AH (10 μM) with and without OmpT or APN inhibitors. (a-b) Confocal images of various bacteria strains including CFT073, UTI89, J96, MRSA, *E. faecalis* and *P. mirabilis* incubated individually with NO–AH (10 μM) in PBS at 37 °C for 2 h, with their fluorescence intensities indicated. (λ_{ex}: 640 nm, λ_{em}: 700/30 nm) Scale bar: 2.5 μm. (c–e) Confocal images of uropathogenic *E. coli* bacteria incubated with NO–AH (10 μM) in the presence and absence of an OmpT inhibitor (Ac-RffRr), and in the presence and absence of an APN inhibitor (Bestatin); CFT073 and UTI89 were incubated with and without the OmpT inhibitor (3.2 mM) for 1 h or APN inhibitor (1.0 mM) for 30 mins first, and then incubate for another 2 h with NO–AH (10 μM) in PBS at 37 °C. (λ_{ex}: 640 nm, λ_{em}: 700/30 nm) Scale bar: 2.5 μm. (f) Confocal images of CFT073 with NO–AH (10 μM) at scale bar of 10 μm and 5 μm. Data presented as means ± SD ($n = 3$).

Moreover, we further selected CFT073 and UTI89, which are typical uropathogenic *E. coli* strains known to cause UTI,[18] to validate the enzyme activity upon treatment with an OmpT inhibitor (e.g. Ac-RffRr).[19] As shown in Figure 2c and 2d, the confocal imaging showed an obvious fluorescence in CFT073 and UTI89 strains upon NO–AH incubation, however, there was significant fluorescence decrease in the presence of an OmpT inhibitor, Ac-RffRr, in the bacterial imaging after treated with NO–AH probe. This further confirms the promising specificity of the NO–AH probe towards bacteria strains expressing OmpT. Likewise, we also validated the specific enzymatic activity of APN by inhibiting APN in CFT073 and UTI89. In Figure 2c and 2e, the fluorescence signal was found to decrease significantly in the presence of APN inhibitor (e.g. Bestatin). Unequivocally, these results demonstrated the necessity of the both proteases working in synergy to specifically activate the molecular probe of NO–AH, for enhanced fluorescence imaging in uropathogenic *E. coli* strains. Such enzyme-specific bacterial imaging can be further quantified with the fluorescence readout for the CFT073 recognition, with the results observed as low as ~10^4 CFU/mL (Figure S8, Supporting Information), comparable to most of the analysis reported previously.[2a,7,20]

Synergistic Enzyme Activation of NO–AH for Localized Imaging in Bacterial Periplasm

In our rational design of NO–AH, one unique section was the bacterial enzymes working in synergy to specifically localize activated fluorescence probe within bacterial bodies. As shown in Figure 2a–d, incubation of NO–AH with OmpT-positive CFT073 strain would lead to a specific bacterial imaging at ~700 nm. Intriguingly, the amplified fluorescence imaging revealed a distinct silhouette formed on the surface of CFT073 (Figure 2f), implying the possibility of well-localized fluorescence in the periplasmic region. Furthermore, we investigated the specific and localized imaging ability of NO–AH in a mixture of live bacterial cultures. Typically, CFT073 was first co-cultured with varying ratios of *Proteus Mirabilis*, a controlled strain with similar morphology but no OmpT, while maintaining a total bacteria count ~10^8 CFU/mL. As shown in Figure 3a, upon incubation with NO–AH (10 μM) with bacterial co-cultures, an increasing trend in fluorescence signal could be clearly observed along with the bacterial co-cultures containing more proportions of CFT073. Similarly, cell cytometry (FCM) analysis was utilized to quantify the increasing fluorescence signals,[21] and more fluorescence corresponding to increasing ratios of CFT073 in bacterial mixtures could be observed. These fluorescence responses further ascertained the imaging selectivity and regional targeting of NO–AH towards CFT073 over *Proteus Mirabilis* in a mixed bacterial environment.

Motivated by these promising discoveries, we then validated if localized bacterial imaging was achievable through the sequential enzymes activity and their distribution within the bacterial cell wall of UPECs to activate NO–AH. To this end, *Proteus Mirabilis* (PM) was first labeled with hoechst (10 μM), followed by co-culturing with OmpT-expressed CFT073, and then incubated with NO–AH (10 μM) for imaging analysis (Figure 3c). The confocal microscopy images in Figure 3d showed a clear bacteria distinction between *Proteus Mirabilis* (PM) and CFT073, whereby the blue signal (hoechst) represents *Proteus Mirabilis*, and the red signals (NO–AH) belong to CFT073, with minimal red signal staining found in *Proteus Mirabilis* (PM). Such responses further confirmed the selectivity and periplasmic-localization of NO–AH towards CFT073 only. Interestingly, a red fluorescence signal surrounding the perimeter of CFT073 was observed (Figure 3d), highlighting the significance of the spatial distribution of both enzymes in trapping the fluorescence signal via the sequential activation of OmpT and APN, so as to contribute the localized bacterial imaging in the periplasm of CFT073.

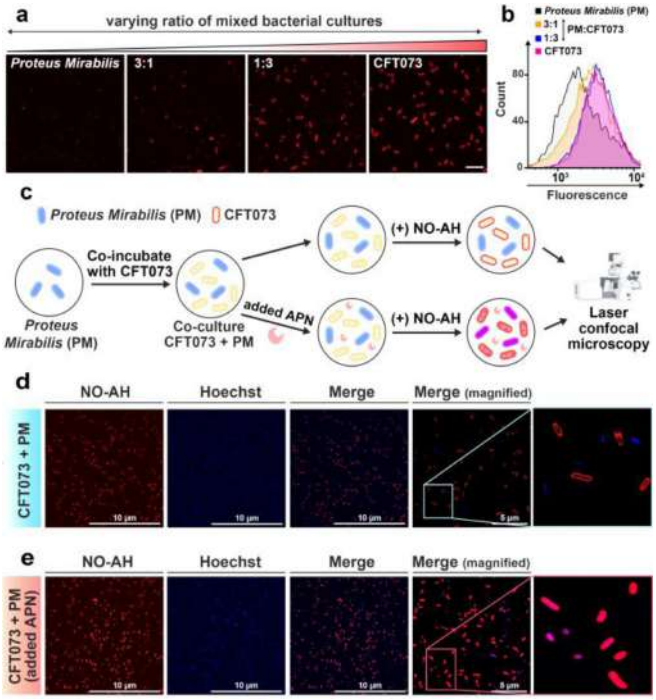

Figure 3. In vitro fluorescence confocal microscopy analysis of the differentiation between live cultures of CFT073 (~10^8 CFU/mL) and *P. mirabilis* (~10^8 CFU/mL). (a) Confocal images of varying ratios co-culture of *P. mirabilis* and CFT073 after incubation with NO–AH (10 μM) for 2 h in PBS at 37 °C; Scale bar: 2.5 μm. (b) FCM analysis of varying ratios of co-culture of *P. Mirabilis* and CFT073 after incubation with NO–AH (10 μM) for 2 h in PBS at 37 °C. (c) Schematic illustration for the investigation of the spatial distribution of dual enzymes in a mixed bacteria. (d) Confocal images of co-culture of hoechst-stained *P. Mirabilis* and CFT073 after incubation with NO–AH (10 μM) for 30 minutes in PBS at 37 °C. (e) Confocal images of co-culture of hoechst- stained *P. Mirabilis* and CFT073, with addition of APN into mixed bacterial envrionment, and then incubation with NO–AH (10 μM) for 30 minutes in PBS at 37 °C (Hoechst: λ_{ex}: 405 nm, λ_{em}: 460/30 nm; NO–AH: λ_{ex}: 640 nm, λ_{em}: 700/30 nm) Scale bar: 10 μm and 5 μm. ($n=3$)

Importantly, to further evaluate the necessity of the spatial location of both enzymes and their impact on localized imaging, we conducted interference experiments to disrupt the spatial distribution of the bacterial enzymes by introducing APN into co-cultured bacterial mixture. Upon the addition of APN (abcam; EC 3.4.11.2) into the bacterial co-cultures, there was an increase in red fluorescence staining across the overall number of bacteria. Unlike the co-culture study without APN addition in Figure 3d, we found that more bacteria, which have been already stained with blue fluorescence, were labelled with red fluorescence (Figure 3e). In this scenario, we believed that OmpT on the outer membrane of CFT073 would first interact with NO–AH to produce R–CyOH. Since the added APN was present in the culture medium, these APN would have cleaved off the arginine residue from R–CyOH to afford the free CyOH leaking into the co-cultured bacterial environment. This resulted in more red fluorescence staining, especially for OmpT-negative *Proteus Mirabilis* (PM), in which significant red bacterial labelling can be observed. As such, the red fluorescence signal could no longer be effectively localized in CFT073 only (Figure 3d and 3e), and there were more fluorescence signals overlap between the red and blue channels, as quantified by the Pearson correlation coefficient value increasing from 0.485 to 0.614 (Figure S9) along with addition of APN into the mixed bacterial environment. This phenomenon further proved that the added APN could induce the diffusion of the free CyOH in mixed bacterial envrionment that eventually stained into *Proteus Mirabilis* (PM), interfering the initial localized imaging of UPECs. These results clearly indicated the rationale that the specific and localization imaging capability of NO–AH is largely influenced by the incorporation of both OmpT and APN located in the different spaces of the UPECs bacterial cell wall.

Furthermore, we also considered the potential interference caused by the presence of abundant metabolic enzymes from the complex cellular environment in a living system. In particular, a commonly used proteolytic enzyme, trypsin, was added into live cultures of CFT073 (OmpT (+)) and *P. Mirabilis* (OmpT (−)) separately, followed by their individual incubation with NO–AH (10 μM). Noteworthily, the addition of trypsin into CFT073 showed a negligible fluorescence change as compared to the NO–AH incubation with CFT073 without trypsin (Figure S10). Moreover, the fluorescence signal of NO–AH demonstrated a consistent response in the presence of both trypsin and its inhibitor (BBI), further validating the minimal influence of metabolic enzymes on UPECs staining. As expected, *P. Mirabilis* with trypsin addition was comparable to the faint fluorescent emission in *P. Mirabilis* without trypsin. These responses indicated the minimal interference of such metabolic enzymes on the specificity of NO–AH towards OmpT-expressing UPECs imaging (Figure S10; Supporting Information). Moreover, throughout the entire imaging studies, the live/dead staining and cellular analysis demonstrated promising biocompatibility of NO–AH, (Figure S11 and S12; Supporting Information), suggesting the potential of our NO–AH probe for selective labelling of OmpT-expressed CFT073 and precise imaging of UTI in vivo.

Locoregional Imaging of UTI in vivo

Driven by effective labeling performance in UTI bacteria and unique merits of fluorescence imaging at NIR window,[22] we further explored the feasibility of enzyme responsive NO–AH to image uropathogenic bacteria caused UTI in living animals. Generally, we first established a mouse model of urinary tract bacterial infection, whereby *E. coli* CFT073 were directly injected into the bladder of female BALB/c mice via the urethra, infecting over prolong time duration.[23] After infection, the number of *E. coli* CFT073 in the mice was measured in the urine, bladder, urethra and kidneys. As shown in Figure S13a, the highest amount of *E. coli* CFT073 was observed at 6 h post-infection, and gradually decreasing over time by expulsion from the body. Meanwhile, the immune response in the

relevant organs were tested and the significantly elevated interleukin-6 levels were observed at 6 h post-infection, signalling an obvious inflammation response induced by bacterial infection in living mice (Figure S13b, Supporting Information). Furthermore, H&E staining (Figure S14, Supporting Information) also showed swelling and shedding of the epithelial cells at the bladder and urethra region, with a large number of bacteria spotted at 6 h post-infection in the bladder (Figure S14; orange circle, Supporting Information), suggesting the successful UTI mouse model established in vivo within a 6 h bacterial infection period for real-time imaging by using NO–AH (Figure 4a to 4c). To monitor the performance and potential fluorescence changes of NO–AH probe in vivo, NO–AH (50 μM) was directly injected into the bladder of the living mice bearing the 6 h infection model, and the mice were imaged immediately under a IVIS Lumina II imaging system at various time points post-NO–AH treatment. Upon in-bladder injection of NO–AH (50 μM) in UTI infected mice, a significant fluorescence increase could be observed which could maintain over a period of 3 hours, compared to the same probe injection into healthy mice (Figure 4d and 4e). Such remarkable observation indicated the feasibility of selective response of NO–AH towards a urinary tract infection. As controls, the fluorophore CyOH (50 μM) alone was also injected directly into the bladder of living mice with or without infection, and the in vivo fluorescent imaging signals were observed to remain relatively consistent for both healthy and infected mice. No apparent fluorescence difference was observed in both the healthy and UTI infected mice (Figure 4d and 4e), featuring the non-selective fluorescence staining from CyOH molecule itself, whereas our dual enzyme responsive NIR NO–AH probe could specifically respond to the UTI environment and realize regional imaging of urinary tract infection in real-time.

Inspired by such promising in vivo imaging studies, we further examined the possibility of NO–AH probe for in vivo UTI imaging upon its intravenous (*i. v.*) injection over a range of time points (Figure 4f). As shown in Figure 4g and 4h, the bladder region of the mice showed an obvious fluorescence enhancement, with the fluorescence signal increasing over 3 hours. As controls, healthy mice were given the same *i. v.* injection of NO–AH and there was no fluorescence enhancement observed across a period of 3 hours. Furthermore, after 4 hours, with the same *i. v.* NO–AH injection, the mice were then sacrificed to visualize the fluorescence in organs. Figure 4g clearly indicated signal confined in the bladder of the infected mice. These results demonstrated that NO–AH can perform real-time imaging for localized monitoring of urinary tract infection in living animals.

Notably, throughout UTI treatment in hospitals, imprecise urine tests can easily lead to the misdiagnosis of UTI that would raise the risk of recurrence and prolong the time for treatment,[6] potentially impacting people in terms of health complications and financial burden caused by medical costs incurred. As such, we investigated the feasibility of our NIR NO–AH probe to sensitively read out the status of UTI caused by UPECs strains. As shown in Figure 4i, after

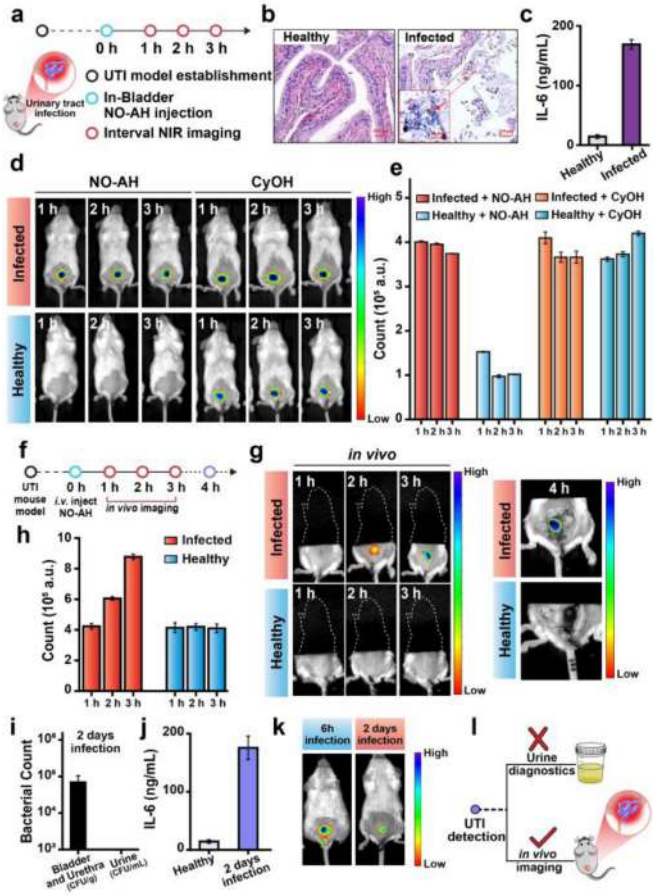

Figure 4. In vivo NIRF imaging of living mice. (a) Schematic illustration of the NIRF imaging of UTI infected mice with in-bladder injection of NO–AH (50 μM) and imaged over different time points. (b–c) H&E staining and IL-6 levels of the bladder and urethra in the healthy and UTI infected mouse after 6 hours of infection. (d–e) NIRF images for UTI infected mice and healthy mice after in-bladder injection of NO–AH (50 μM) and CyOH (50 μM) separately, and their corresponding fluorescence signals. λ_{ex}: 660 nm, λ_{em}: 710 nm. (f) Illustration of the NIRF imaging of UTI infected mice with *i. v.* injection of NO–AH (50 μM) and imaged over different time points. (g–h) NIRF images for UTI infected mice and healthy mice with *i. v.* injection of NO–AH (50 μM); and their corresponding fluorescence signals. λ_{ex}: 660 nm, λ_{em}: 710 nm (i) Bacterial count of CFT073 present in the urine, bladder and urethra after 2 days of bacterial infection. (j) IL-6 levels of healthy and recurrent UTI mice after 2 days bacterial infection (k) NIRF imaging for 6 h and 2 days UTI infected mice with NO–AH injection (50 μM). λ_{ex}: 660 nm, λ_{em}: 710 nm (l) Scheme of detecting UTI in vivo. Data presented as means ± SD ($n = 3$).

2 days CFT073 UPECs infection in living mice, there was no bacteria detectable in the urine sample of the mice, whereas ex vivo tissue infection analysis showed that a significant amount of CFT073 (~10^5 CFU/g) was found remaining in the bladder and urethra regions. Meanwhile, the IL-6 levels clearly indicated an immune response after 2 days of CFT073 infection (Figure 4j). These observations implied that a bacterial infection was still occurring in the mice, suggesting the possibility of UTI misdiagnosis caused by the imprecision in routine urine test. While, in vivo imaging by administration of NO–AH into living mice with the 2 days

CFT073 infection demonstrated an obvious fluorescence signal in the bladder and urethra, which was similar to that of the fluorescence observed in the bladder and urethra of the 6 h CFT073 infected mice (Figure 4k). These findings proved that NO–AH could directly visualize the status of UTI in vivo whereby such readout may not be possible in normal urine samples (Figure 4l).

Conclusion

In conclusion, we have developed a first-in-class near-infrared fluorescence probe (NO–AH) for real-time and localized bacterial imaging of a urinary tract infection in vitro and in vivo. The NIR probe specifically triggered by a collaborative activation of two membrane enzymes of OmpT and APN at different intracellular spaces could trap the activated fluorescence of NO–AH within periplasmic region, thereby establishing the feasibility of localized bacterial imaging in UPECs strains and in a mixed bacterial environment. Such unique probe design demonstrated the exceptional feature of bacterial surface proteases in synergy for rapid and locoregional identification of UPECs strains responsible for UTI infection that could minimize the possibility of misdiagnosis deriving from urine sample analysis, providing new insights on unprecedented developments of timely and precise UTI diagnosis for effective antimicrobial therapeutics management in future.

Supporting Information

The authors have cited additional references within the Supporting Information.[24]

Acknowledgements

This work is supported by MOE Tier 1 RG4/22, RG6/20, RG69/21, MoE AcRF Tier 1 Theme RT7/22, A*Star SERC A1983c0028, A20E5c0090, awarded at Nanyang Technological University (NTU), the Major State Basic Research Development Program of China (2023YFB3810000), National Natural Science Foundation of China (NSFC) (No. 51929201, 22007083, 81925019, U22A20333). We would like to sincerely thank Professors Kimberley Kline and Yuan Qiao from Nanyang Technological University for donating bacteria strains used in this study.

Conflict of Interest

The authors declare no conflict of interest.

Data Availability Statement

The data that support the findings of this study are available in the supplementary material of this article.

Keywords: Urinary tract infections · Bacterial membrane enzymes · Fluorescence imaging · NIR · Peptide probes

[1] a) A. L. Flores-Mireles, J. N. Walker, M. Caparon, S. J. Hultgren, *Nat. Rev. Microbiol.* **2015**, *13*, 269–284; b) L. K. McLellan, D. A. Hunstad, *Trends Mol. Med.* **2016**, *22*, 946–957.
[2] a) L. Mendive-Tapia, D. Mendive-Tapia, C. Zhao, D. Gordon, S. Benson, M. J. Bromley, W. Wang, J. Wu, A. Kopp, L. Ackermann, M. Vendrell, *Angew. Chem. Int. Ed. Engl.* **2022**, *61*, e202117218; b) R. D. Klein, S. J. Hultgren, *Nat. Rev. Microbiol.* **2020**, *18*, 211–226.
[3] G. R. Nielubowicz, H. L. Mobley, *Nat. Rev. Urol.* **2010**, *7*, 430–441.
[4] N. Sihra, A. Goodman, R. Zakri, A. Sahai, S. Malde, *Nat. Rev. Urol.* **2018**, *15*, 750–776.
[5] a) M. Davenport, K. E. Mach, L. M. D. Shortliffe, N. Banaei, T. H. Wang, J. C. Liao, *Nat. Rev. Urol.* **2017**, *14*, 296–310; b) E. Yan, G. Kwek, N. S. Qing, S. Lingesh, B. Xing, *ChemPlusChem* **2023**, *88*, e202300009.
[6] a) S. W. C. Koh, T. S. M. Ng, V. W. K. Loh, J. C. Goh, S. H. Low, W. Z. Tan, H. C. Wong, P. Durai, L. J. Sun, D. Young, P. A. Tambyah, *Antimicrob. Resist. Infect. Control* **2023**, *12*, 73; b) M. C. Goebel, B. W. Trautner, L. Grigoryan, *Clin. Microbiol. Rev.* **2021**, *34*, e0000320; c) A. Capstick, F. Palermo, K. Zakka, N. Fletcher-Lloyd, C. Walsh, T. Cui, S. Kouchaki, R. Jackson, M. Tran, M. Crone, K. Jensen, P. Freemont, R. Vaidyanathan, M. Kolanko, J. True, S. Daniels, D. Wingfield Cr, T. Group, R. Nilforooshan, P. Barnaghi, *NPJ Digit Med* **2024**, *7*, 11.
[7] a) S. Meile, J. Du, S. Staubli, S. Grossmann, H. Koliwer-Brandl, P. Piffaretti, L. Leitner, C. I. Matter, J. Baggenstos, L. Hunold, S. Milek, C. Guebeli, M. Kozomara-Hocke, V. Neumeier, A. Botteon, J. Klumpp, J. Marschall, S. McCallin, R. Zbinden, T. M. Kessler, M. J. Loessner, M. Dunne, S. Kilcher, *Nat. Commun.* **2023**, *14*, 4336; b) A. van der Zee, L. Roorda, G. Bosman, J. M. Ossewaarde, *PLoS One* **2016**, *11*, e0150755; c) R. Pandey, D. Chang, M. Smieja, T. Hoare, Y. Li, L. Soleymani, *Nat. Chem.* **2021**, *13*, 895–901; d) S. Park, K. Park, H. Cho, J. Kwon, K. S. Kim, H. Yang, *Anal. Chem.* **2022**, *94*, 4756–4762.
[8] S. Gutkin, R. Tannous, Q. Jaber, M. Fridman, D. Shabat, *Chem. Sci.* **2023**, *14*, 6953–6962.
[9] O. Shelef, T. Kopp, R. Tannous, M. Arutkin, M. Jospe-Kaufman, S. Reuveni, D. Shabat, M. Fridman, *J. Am. Chem. Soc.* **2024**, *146*, 5263–5273.
[10] a) S. E. Wood, G. Sinsinbar, S. Gudlur, M. Nallani, C. F. Huang, B. Liedberg, M. Mrksich, *Angew. Chem. Int. Ed. Engl.* **2017**, *56*, 16531–16535; b) X. L. He, Q. Wang, L. Peng, Y. R. Qu, S. Puthiyakunnon, X. L. Liu, C. Y. Hui, S. Boddu, H. Cao, S. H. Huang, *Pathog Dis* **2015**, *73*.
[11] a) G. Sinsinbar, S. Gudlur, S. E. Wood, G. Ammanath, H. U. Yildiz, P. Alagappan, M. Mrksich, B. Liedberg, *Angew. Chem. Int. Ed. Engl.* **2020**, *59*, 18068–18077; b) Y. Hu, L. Zhang, J. Chen, J. Yao, H. Jin, P. Yang, *Anal. Chem.* **2020**, *92*, 732–739; c) M. J. Olsen, D. Stephens, D. Griffiths, P. Daugherty, G. Georgiou, B. L. Iverson, *Nat. Biotechnol.* **2000**, *18*, 1071–1074.
[12] a) X. Wen, W. Zeng, J. Zhang, Y. Liu, Y. Miao, S. Liu, Y. Yang, J. J. Xu, D. Ye, *Angew. Chem. Int. Ed. Engl.* **2024**, *63*, e202314039; b) Y. Chen, P. Pei, Y. Yang, H. Zhang, F. Zhang, *Angew. Chem. Int. Ed. Engl.* **2023**, *62*, e202301696.
[13] Z. Cheng, E. J. Thompson, L. Mendive-Tapia, J. I. Scott, S. Benson, T. Kitamura, A. Senan-Salinas, Y. Samarakoon, E. W. Roberts, M. A. Arias, J. Pardo, E. M. Galvez, M. Vendrell, *Angew. Chem. Int. Ed. Engl.* **2023**, *62*, e202216142.

[14] a) A. A. L. Gay, B. W. Matthews, *Biochemistry* **2008**, *47*, 5303–5311; b) D. Chandu, D. Nandi, *Microbiology (Reading)* **2003**, *149*, 3437–3447.
[15] a) J. Weng, Y. Wang, Y. Zhang, D. Ye, *J. Am. Chem. Soc.* **2021**, *143*, 18294–18304; b) T. C. Do, J. Lau, C. Sun, S. Liu, K. T. Kha, S. T. Lim, Y. Y. Oon, Y. P. Kwan, J. J. Ma, Y. Mu, X. Liu, T. J. Carney, X. Wang, B. Xing, *Sci. Adv.* **2022**, *8*, eabq2216; c) J. Fang, Y. Zhao, A. Wang, Y. Zhang, C. Cui, S. Ye, Q. Mao, Y. Feng, J. Li, C. Xu, H. Shi, *Anal. Chem.* **2022**, *94*, 5149–5158.
[16] I. Desloges, J. A. Taylor, J. M. Leclerc, J. R. Brannon, A. Portt, J. D. Spencer, K. Dewar, G. T. Marczynski, A. Manges, S. Gruenheid, H. Le Moual, J. L. Thomassin, *MicrobiologyOpen* **2019**, *8*, e915.
[17] Z. Wang, T. D. Cong, W. Zhong, J. W. Lau, G. Kwek, M. B. Chan-Park, B. Xing, *Angew. Chem. Int. Ed. Engl.* **2021**, *60*, 16900–16905.
[18] K. Schaale, K. M. Peters, A. M. Murthy, A. K. Fritzsche, M. D. Phan, M. Totsika, A. A. B. Robertson, K. B. Nichols, M. A. Cooper, K. J. Stacey, G. C. Ulett, K. Schroder, M. A. Schembri, M. J. Sweet, *Mucosal Immunol.* **2016**, *9*, 124–136.
[19] V. Hritonenko, C. Stathopoulos, *Mol. Membr. Biol.* **2007**, *24*, 395–406.
[20] L. Zhang, B. Wang, G. Yin, J. Wang, M. He, Y. Yang, T. Wang, T. Tang, X. A. Yu, J. Tian, *Int. J. Nanomed.* **2022**, *17*, 3723–3733.
[21] a) J. Aw, F. Widjaja, Y. Ding, J. Mu, L. Yang, B. Xing, *Chem. Commun. (Camb.)* **2017**, *53*, 3330–3333; b) Q. Z. Jaber, M. Bibi, E. Ksiezopolska, T. Gabaldon, J. Berman, M. Fridman, *ACS Cent. Sci.* **2020**, *6*, 1698–1712.
[22] a) Y. Chen, P. Pei, Z. Lei, X. Zhang, D. Yin, F. Zhang, *Angew. Chem. Int. Ed. Engl.* **2021**, *133*, 15943–15949; b) Z. Zheng, A. Duan, R. Dai, Y. Li, X. Chen, Y. Qin, S. Ren, R. Li, Z. Cheng, R. Zhang, *Small* **2022**, *18*, e2201179; c) H. Chen, L. Liu, K. Qian, H. Liu, Z. Wang, F. Gao, C. Qu, W. Dai, D. Lin, K. Chen, H. Liu, Z. Cheng, *Sci. Adv.* **2022**, *8*, eabo3289; d) O. Redy-Keisar, E. Kisin-Finfer, S. Ferber, R. Satchi-Fainaro, D. Shabat, *Nat. Protoc.* **2014**, *9*, 27–36.
[23] C. S. Hung, K. W. Dodson, S. J. Hultgren, *Nat. Protoc.* **2009**, *4*, 1230–1243.
[24] a) R. Yan, Y. Hu, F. Liu, S. Wei, D. Fang, A. J. Shuhendler, H. Liu, H.-Y. Chen, D. Ye, *J. Am. Chem. Soc.* **2019**, *141*, 10331–10341; b) V. Hritonenko, C. Stathopoulos, *Mol. Membr. Biol.* **2007**, *24*, 395–406.

Manuscript received: April 10, 2024
Accepted manuscript online: June 3, 2024
Version of record online: ■■, ■■

Research Article

Fluorescent Probes

E. Y. H. Xin, G. Kwek, X. An, C. Sun, S. Liu, N. S. Qing, S. Lingesh, L. Jiang, G. Liu,* B. Xing* **e202406843**

Enzymes in Synergy: Bacteria Specific Molecular Probe for Locoregional Imaging of Urinary Tract Infection in vivo

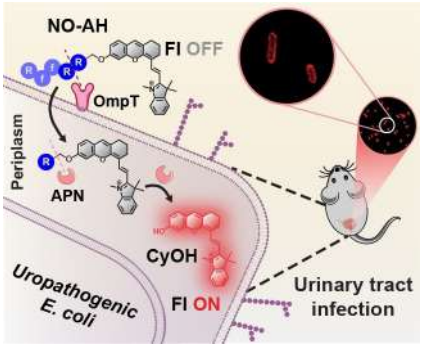

We developed a first-in-class near-infrared uropathogenic *E. coli* (UPECs) peptide fluorescent probe (NO–AH) capable of specifically targeting UPECs via the collaborative response of bacterial enzymes (OmpT and APN), enabling locoregional imaging of urinary tract infections both in vitro and in vivo, opening new avenues for timely and precise UTI diagnosis.